RESEARCH ARTICLE

Check for updates

Novel self-assembling cyclic peptides with reversible supramolecular nanostructures†

Maria Gessica Ciulla, [ID] [a] Federico Fontana, [ab] Roberto Lorenzi, [ID] [c]
Amanda Marchini, [ab] Luca Campone, [d] Ehsan Sadeghi, [c] Alberto Paleari, [ID] [c]
Sara Sattin [ID] [e] and Fabrizio Gelain [ID] *[ab]

Self-assembly peptides (SAPs) are an important class of hydrogels used in nanomedicine for tissue repair and neural regeneration. Due to their unique properties, SAPs may be used in a wide range of applications but some limitations, such as low bioavailability and rapid hydrolysis degradation, need to be overcome. Here, we describe the synthesis and characterization of two novel cyclic SAPs without the use of D/L-alternating amino acids, showing a reversible transition of their supramolecular nanostructures, from nanotubes/nanofibers into nanovesicles/nanospheres. The investigation, characterization and optimization are performed using atomic force microscopy (AFM), attenuated total reflectance-Fourier transform infrared (ATR-FTIR) spectroscopy, Raman analysis, circular dichroism (CD), and rheology measurements. Also, *in vitro* cell viability assays show negligible toxicity of the representative optimized cyclic SAP towards human neural stem cells (hNSCs). Our results suggest that linear SAP theoretical background can be applied to develop cyclic SAPs, with important implications in the scalable fabrication of inter-changeable nanostructures, as well as for biomedical applications, including tissue regeneration, drug-delivery, drug-design, sensing, imaging, and size selectivity.

Introduction

Proteins and peptides are the most abundant mediators of all living cell systems.[1] Naturally occurring and synthetic peptides are in high demand for a wide range of applications, from regenerative medicine[2] to drug discovery and chemical biology.[3] Recently, cyclic peptides have emerged as promising compounds to overcome some typical weaknesses of peptides, such as low oral bioavailability, short half-life, and low membrane penetration.[4] The ability to spontaneously self-organize, through self-assembly, confers unique features to peptides. SAPs are an attractive class of scaffolds with huge potential in biomedical fields. The principles of self-assembly concern hierarchical organization that, thanks to supramolecular interactions rather than covalent interactions, drives the formation of well-ordered nanostructures.[5,6] Natural

EAK16 (AEAEAKAKAEAEAKAK)[7,8] from yeast protein, and the synthetic derivative RADA16 (RADARADARADARADA)[9] are linear SAPs that self-assemble in aqueous solutions into stable β-sheets, and form hydrogels with high water content (≥99% w/v water). Both were used as models to design different optimized versions of new SAPs. Indeed, by strategical fine-tuning, these building blocks can be bottom–up designed for the fabrication of diverse architectures. However, the different self-assembly propensity of linear and respective cyclic peptides has not been completely explored.[10] The common strategy to form self-assembling cyclic peptides and peptide amphiphile nanotubes is the use of alternating D- and L-amino acids, which are stabilized by stacking intermolecular hydrogen bonds. Biological tubular assemblies, such as protein aquaporin[11] or β-tubulin,[12] may inspire the intriguing potential functions of these systems. Since the discovery of carbon nanotubes,[13,14] tubular structures with an internal pore have enabled researchers to mimic biological channels or to design nanoscale devices for (bio)sensor technology,[15] for size-selective gates,[16] as dynamic transporters,[17] as cell penetrating peptides,[18,19] for drug delivery[20] and to influence the lipidic distribution in cell membranes.[21] Over the last twenty years, low molecular weight hydrogelators, and in general peptide-based hydrogels, have attracted attention thanks to their high potential, *i.e.* the biocompatibility and the propensity to form organogels (useful in molecule absorption to remove pollutants from water).[22] Some emerging applications of dipeptide hydrogels,

a Institute for Stem-Cell Biology, Regenerative Medicine and Innovative Therapies, IRCCS Casa Sollievo della Sofferenza, 71013 San Giovanni Rotondo, Italy. E-mail: f.gelain@css-mendel.it

b Center for Nanomedicine and Tissue Engineering (CNTE), ASST Grande Ospedale Metropolitano Niguarda, 20162 Milan, Italy

c Department of Materials Science, University of Milano-Bicocca, 20125 Milan, Italy

d Department of Biotechnology and Biosciences, University of Milano-Bicocca, 20125 Milan, Italy

e Department of Chemistry, University of Milan, 20133 Milan, Italy

† Electronic supplementary information (ESI) available. See DOI: https://doi.org/10.1039/d3qm00198a

such as Fmoc-FF-OH and Fmoc-RGD-OH, involved 3D-cell scaffolds for the improvement of the growth of human dermal fibroblasts.[23] These studies supported the interest in the advancement of self-assembled bioactive compounds to explore cell therapy, tissue engineering, and cell biology.

A peculiar and interesting behavior of some cyclic peptides is the reversible transition among different nanostructures, *e.g.* between nanotubes and vesicle-like structures, which may serve to devise other complex engineering systems.[24] As reported in the literature, to date, cyclic peptide nanotubes (*i.e.* amphiphilic nanotubes[25]) were built mostly from alternated L/D amino acids to form large nanosheets with two-dimensional self-assembly properties.[26] In this work, two cyclic SAPs, cyclo-LDLK12 (cyclo-LDLKLDLKLDLK) and cyclo-FAQ-LDLK12 (cyclo-FAQRVPPGG-GLDLKLDLKLDLK), containing amino acids exclusively with L configuration were investigated. The lead sequence was derived from a well-known linear SAP, LDLK12,[27,28] widely used in regenerative medicine applications,[2,29,30] and already reported in our previous studies. It should be noted that various approaches for peptide cyclization are known, but a single ideal method for all peptides is not available. The cyclic SAPs here described were synthesized through a head-to-tail optimized cyclization. Moreover, cyclo-LDLK12 is proposed as a model for the fabrication of novel cyclic SAPs featuring reversible shape transition of disassembly and reassembly depending on solvent conditions. These supramolecular changes are trigged by pH exchange and may be useful to define their application in various physiological environments. Furthermore, molecular dynamics (MD) simulations elucidated the molecular mechanisms regulating self-assembly. MD atomistic simulations revealed that the cyclic peptides adopt arrangements compatible with the alpha-helix and beta-sheet domains. The investigation with Morphoscanner of both atomistic and coarse-grained MD simulations pointed out the emergence of disordered structural domains when SAPs are embedded in a neutral solvent. Morphological characterization of the cyclic SAPs demonstrated a versatile self-assembling aggregation of reversible and tunable nanostructures. The secondary structure of cyclo-LDLK12 and cyclo-FAQ-LDLK12 showed, both empirically (Raman and FTIR spectroscopy) and in MD experiments, an unusual intramolecular β-content. Additionally, rheological evaluation of the functionalized cyclo-FAQ-LDLK12 yielded a stiffer and more resilient hydrogel compared to the respective linear SAP. Finally, cyclo-FAQ-LDLK12 was tested through *in vitro* experiments to evaluate the viability of hNSCs, demonstrating negligible cytotoxicity of cyclo-LDLK12-based peptides.

Results and discussion

Head-to-tail cyclization and optimization

It is well-proven that linear peptide hydrogels are readily hydrolyzed by enzymatic proteolysis in physiological conditions. Cyclization can play a crucial role as it improves stability under harsh conditions,[31] and it may enhance the therapeutic potential of peptide-based molecules. Still, peptide cyclization is not easily accessible due to the formation of secondary products. We

selected the peptide sequence to be cyclized starting from well-known and deeply characterized linear self-assembling peptides: pure self-assembling peptide LDLK12 (Ac-LDLKLDLKLDLK-CONH$_2$),[27,32] and its functionalized version FAQ-LDLK12 (FAQRVPPGG-GLDLKLDLKLDLK-CONH$_2$), bestowed with biomimetic properties triggering neural stem cell differentiation *in vitro*[27,32] and nerve regeneration *in vivo*.[33] LDLK12 is a non-functionalized backbone with a strong spontaneous propensity to self-assemble in ordered structures featured by cross-β nanofibers.[32] It is a short peptide characterized by L-amino acids suitable for cell-based therapies.[33] The 2-CTC resin was used to obtain a free –COOH terminal group: as shown in Scheme S1 (ESI†) step (1) of the synthesis design proceeds on microwave-assisted Fmoc-solid phase peptide synthesis to give intermediate 2 which in the presence of mild acidic conditions, is cleaved from the resin without affecting the side chain protecting groups (3). Then, the head-to-tail cyclization fostered an amide bonding due to condensation between the first residue (an amino functionality, N-terminus) and the last residue (a carboxylate group, C-terminus). Herein, as a part of our investigations, we developed an efficient method to obtain cyclo-LDLK12 in a satisfactory overall yield (56%). The optimization study involved the survey of different coupling conditions (Table S1, entries 1–4, ESI†) for the solution cyclization of the dodecapeptide.[34,35] Indeed, as it is generally known,[36,37] peptide intramolecular ring-closures often proceed under the competition of secondary reactions,[38] such as cyclic dimerization, dimerization, and polymerization. Interestingly, following resin cleavage, the best solution head-to-tail cyclization yield (75%) was obtained in the presence of *N,N*-diisopropylethylamine (DIPEA) with slow addition of benzotriazol-1-yloxytripyrrolidinophosphonium hexafluorophosphate (PyBOP), and hydroxybenzotriazole (HOBt) as coupling reagents (Table S1, entry 4, ESI†). The reaction was performed under diluted conditions and under a longer time (6 hours) to overcome the difficulty to cyclize a terminal Lys(Boc) residue.[39] The other reaction conditions gave low or moderate yields (Table S1, entries 1–3, ESI†). Afterwards, fully deprotected peptide cyclo-LDLK12 was used for further characterization.

Morphological characterization

To investigate the nanostructural features we examined atomic force microscopy (AFM) images of cyclo-LDLK12 at various pH values. The images revealed controlled self-assembly of specific objects obtained by tuning the solution pH. Fig. 1 shows the rare transformation of spherical-like shapes into tubular structures. It was observed that the self-assembled nanostructures modification is a reversible process under repeated cycles of pH transitions. The laps, started by reaching basic conditions (pH ∼ 10), firstly revealed spherical objects with a multiplicity of diameters (from 18 to 324 nm), suggesting that an ordered aggregation of elemental units was taking place. At pH 7, AFM images showed a dynamic transition of the morphology into nanotubes/nanofibers with two main averages in height (0.80 ± 0.01 nm; 1.66 ± 0.77 nm) and width (46.85 ± 0.58; 84.90 ± 0.77) distributions (Fig. S1b, ESI†).
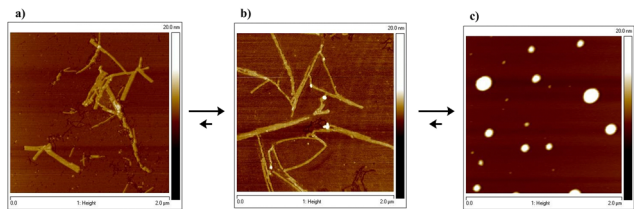
Fig. 1 AFM analysis of self-assembled nanostructure of cyclo-LDLK12 under different pH conditions. (a) Images of linear nanostructures at pH 2; (b) images of linear nanostructures at pH 7; and (c) images of round-shaped aggregates at pH 10.

Stronger acidic conditions (pH ∼ 2, Fig. S1a, ESI†) did not alter the height and width profiles of the detected peptide nanostructures. The curious formation of objects identified as vesicles/nanospheres at pH 10 exhibited different diameters with two main width averages of 113.38 ± 1.61 nm and 221.27 ± 1.99 nm (Fig. S1c, ESI†). The formation of spherical objects under basic conditions suggests that cyclo-LDLK12 self-assembles in supramolecular aggregates with a pH-dependent process.[40] We considered that the shape-transition phenomena act through a type of "domino-reaction" wherein a sufficient free energy of self-assembly drives the 2D supramolecular aggregation. Such mechanism is in agreement with the theoretical model proposed by Yan *et al.*[24]

ATR/FT-IR experiments

In FT-IR experiments (Fig. 2a), amide regions were studied at different pH of sample conditions. We focused on the amide I (1700–1600 cm^{-1}) to investigate the C=O stretching vibration of the peptide bond, which is particularly sensitive to the presence of β-sheets content. It is important to note that, under the tested pH conditions, hydrogens of the acceptor and donor amide groups involved in the H-bonding could exchange.[41,42]

Deconvolution procedures, obtained after second derivatives calculations, were performed to resolve the overlapping bands, yielding detailed structural information. Furthermore, all spectra show the peak at ∼1394 cm^{-1} that is associated with the C–N stretching bond (Fig. 2).[43]

Fig. 2aI and aII, respectively, pH 2 and pH 7, showed the presence of the typical absorption bands of intermolecular antiparallel β-sheets at ∼1618 cm^{-1} and ∼1692 cm^{-1}. At neutral pH, peaks revealed a predominance of unusual β-sheet periodicity (∼1636 cm^{-1}, Fig. 2aII) for twelve-residue cyclic peptides,[44] probably due to a *trans–trans* isomer content related to strongly hydrogen bonded carbonyl.[45] In contrast, a pH exchange seems to induce a conformational isomerization of cyclic amides.[46]

A broad component in the amide II region, described in Fig. 2aI (∼1546 cm^{-1}) and in Fig. 2aIII (∼1583 cm^{-1} and ∼1546 cm^{-1}), was observed and assigned to random coil structures.

According to the literature,[47,48] the component band in the high-frequency amide I region (>1660 cm^{-1}) could be associated to β-turns (pH 10, Fig. 2aIII). Indeed, the FTIR spectra of cyclic peptides featuring H-bonded β- and γ-turns were found to show acceptor bands in the β-turn band region (1655–1675 cm^{-1}).[24]

In agreement with AFM results (Fig. 1 and Fig. S1, ESI†) and Raman experiments (Fig. 2b), we can conclude that vibrations
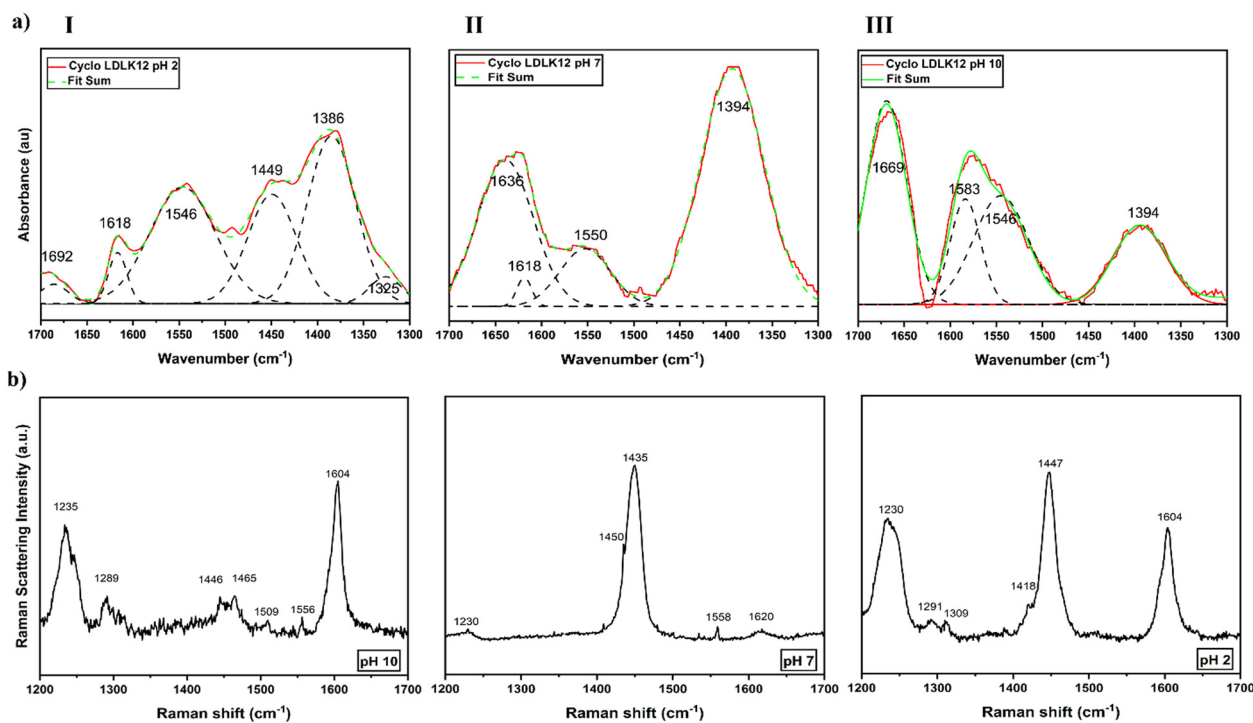

Fig. 2 Spectroscopy characterization of cyclo-LDLK12 at pH 2 (I), pH 7 (II) and pH 10 (III). (a) ATR/FTIR absorption spectra with respective deconvolutions of cyclo-LDLK12 under different pH conditions. Peak deconvolution was performed to determine the composition of the secondary structure under a given condition. (b) Raman spectra of the tested samples.

of cyclo-LDLK12 generally adopted an antiparallel pleated β-sheet conformation.

ATR/FTIR absorption spectra with respective deconvolutions of cyclo-LDLK12 under different pH conditions. Peak deconvolution was performed to determine the composition of the secondary structure under a given condition. (b) Raman spectra of the tested samples.

Raman spectroscopy

Raman spectra of cyclo-LDLK12 at different pH were investigated in the amide I (1600–1680 cm^{-1}), amide II ($\sim$1550 cm^{-1}), and the amide III (1200–1340 cm^{-1}) regions (Fig. 2b). Amide I band shows the C=O stretching, whereas amide II and amide III describe a combination of CN stretching and NH bending.

Spectra collected at different pH show strong differences in the amide regions reflecting the propensity of the peptide to self-assemble in different ways according to the environmental conditions. At pH $\sim$ 2 the Raman spectrum is characterized by two peaks at $\sim$1230 cm^{-1} and 1604 cm^{-1}, typical of peptides with antiparallel β-turns secondary structures,[49] and a third peak at 1450 cm^{-1} associated with the C$_\alpha$–H bending bands. Under neutral conditions the two bands relative to antiparallel β-turns are suppressed, but still detectable, while the main band arises from skeletal carbon bending. In contrast, at pH 10 the C$_\alpha$–H bending is suppressed, but the two bands relative to antiparallel β-turns are still present. This outcome is indicative of a peptide bond conformation in which there is a decoupling of C$_\alpha$–H bending to C–N stretching and N–H bending. Moreover, at pH $\sim$ 10 we register a small increase of a band at about 1290 cm^{-1}.[50] This band is related either to β-turns not in antiparallel configuration or to unordered secondary structures. The very low signal from C$_\alpha$–H is indeed indicative of unfolded conformations. Thus, in accordance with the globular structures observed in AFM images, at higher pH (basic conditions, Fig. 2bIII) the aggregation tends to loosen their inter-ring bond strength. These aspects corroborate the structural evolution of peptides from ordered fibril structures with stronger mechanical properties to unordered rounded structures when passing from an acidic to a basic environment.

The presence of β-sheets aggregation was, also, confirmed by the ThT-binding assay (Fig. 3a). As the benzothiol dye ThT binds β-sheet-rich structures (without binding amorphous aggregates), this colorimetric test was used to detect the β-content in cyclo-LDLK12. The results were compared to the corresponding linear LDLK12, which is a well-characterized self-assembling peptide with a strong self-assembly propensity, and a high β-sheet content.

The cyclic version, although of minor intensity (probably due to the constrained form), showed the interaction between the benzothiol dye and the β-secondary structure in the ThT assay. The ThT assay resulted in high fluorescence levels showing the typical emission signal at 482 nm. Positive and negative peaks, 197 and 216 nm respectively, in CD experiments (Fig. 3b) showed the predominance of antiparallel β-sheets content in cyclo-LDLK12 at pH 7 and pH 2. The presence of
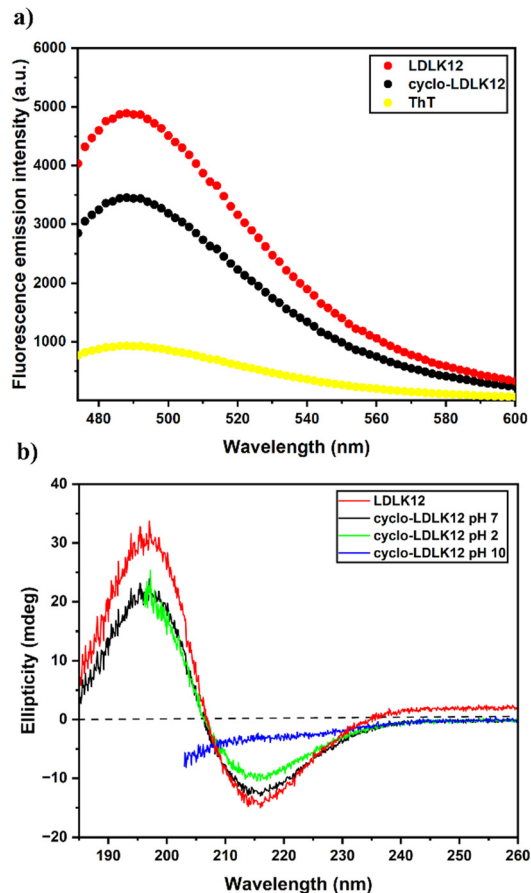

Fig. 3 (a) ThT binding assay and (b) far-UV spectra analysis by CD experiments of cyclo-LDLK12 in comparison with its linear counterpart LDLK12.

random coil formation (CD band at 200 nm) under basic conditions (pH 10) was in agreement with FTIR results.[51]

Molecular dynamic simulations

Molecular dynamics simulations, both atomistic and coarse-grained (CG), have been used in combination with Morphoscanner[52] for studying the self-assembling process of cyclic peptides, adopting a similar protocol to that adopted for other classes of peptides.[53,54] The atomistic molecular dynamics simulations of the cycle peptides unveiled conformational heterogeneity (Fig. 4a). Indeed, Ramachandran's plots highlighted the distributions of and ψ and φ angles in the range from −120° to −60° and from −120° to 180°, respectively. On one hand, the distributions of ψ angles between −120° and −60° and φ angles between −120° and 0° correspond to α-helix conformations. On the other hand, the distributions of ψ angles between −120° and −60° and φ angles between 60° and 180° correspond to β-sheet conformations. The MD simulations of octamer cyclic peptide systems unveiled similar tendencies, as shown in the Ramachandran plots in Fig. 4b. These features affect the self-assembling process, as highlighted by Morphoscanner shift profiles. Indeed, cyclic peptides tend to align in antiparallel β-sheets within globular aggregates. Such considerations remain unchanged
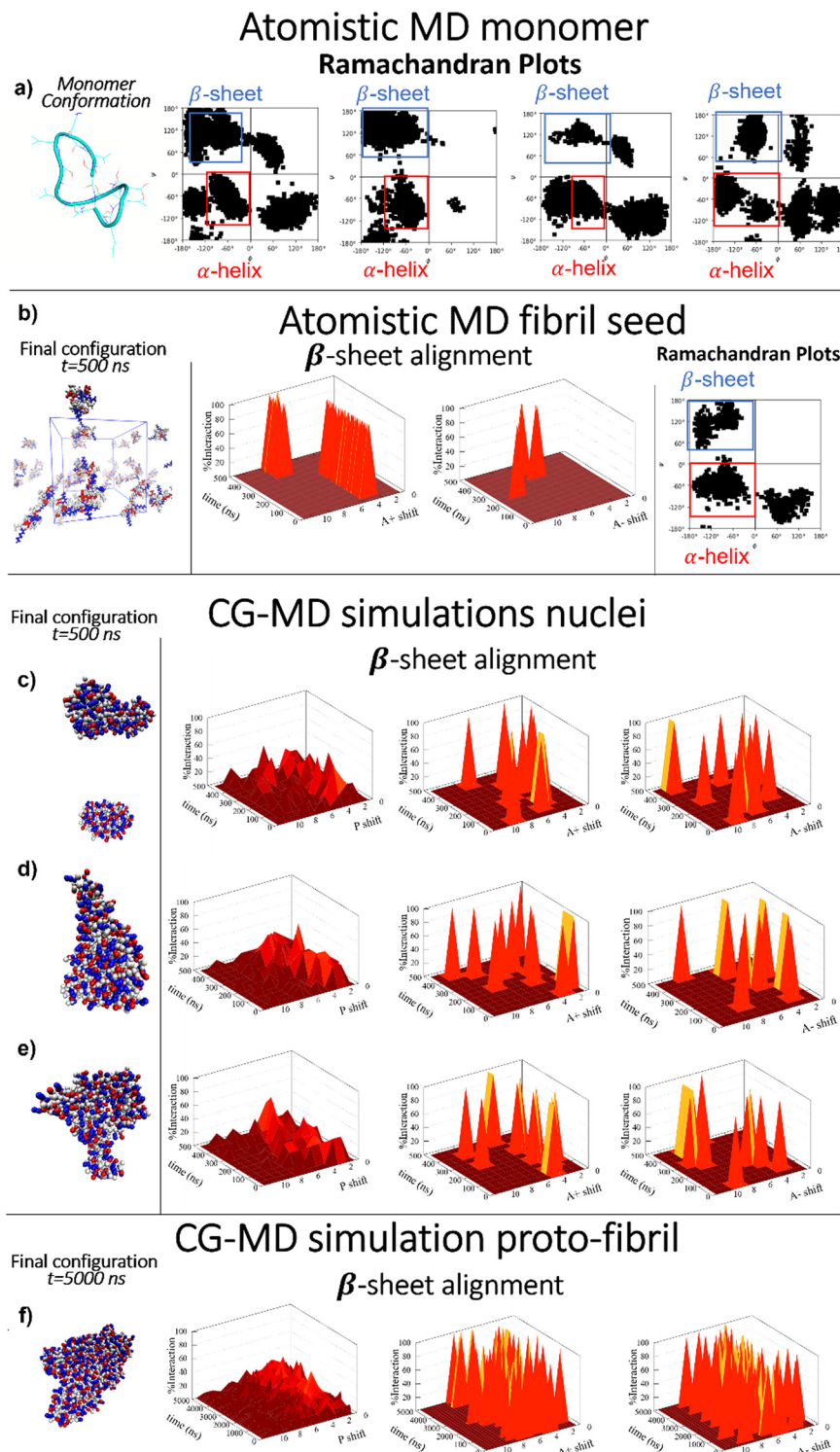
Fig. 4 Cyclo-LDLK12 SAP MD simulations. (a) The UA-MD simulations of the monomers unveil a huge heterogeneity in the cyclo-LDLK12 conformations. Indeed, the Ramachandran plot shows different distributions of ψ and ϕ angles, both compatible with α-helix and β-sheet conformations. (b) The UA-MD simulations of the 8-mer cyclo-LDLK12 SAP corroborate the results of the conformational analysis of the monomers. In addition, the UA-MD simulations of cyclo-LDLK12 8-mers unveil a preferential antiparallel alignment among the β-strands. (c–e) The CG-MD simulations of the 40-mer cyclo-LDLK12 SAPs returned conflictual interpretations about the preferential alignment among the β-strands. In addition, the shape of the macromolecular aggregates is rounded. (f) Instead, the CG-MD simulations of the 100-mer cyclo-LDLK12 SAPs unveiled that the β-strands are mainly antiparallely aligned, nonetheless the shape of the aggregate is still rounded.

when considering the CG-MD simulation of fibril nuclei (Fig. 4c–e). Indeed, the analysis of Morphoscanner shift profiles pointed to an antiparallel alignment within β-sheet-rich peptide clusters. Then, CG-MD simulation of cyclic peptide proto-fibrils identified analogous tendencies (Fig. 4f). The dodecapeptide cyclo-LDLK12 can be considered as the first example of a cyclic self-assembling peptide designed from linear SAPs.

Cyclo-LDLK12 is characterized by tunable self-assembly without using the typical alternated D/L-chiral amino acid sequence,[55,56] enabling the formation of reversible supramolecular architectures in response to external stimuli, such as pH shifts. This model introduces a novel strategy to develop cyclic peptide-based self-assembly peptide systems that may serve as supramolecular materials for different applications as immunosuppressants, antibiotics, antivirals, or anticancer drugs.[57–59] However, its poor solubility in water prevented the formation of stand-alone hydrogels with mechanical properties suited for biotechnology applications, thus suggesting that some optimization still had to be done.

Functionalized cyclic self-assembling peptide

The understanding of the phenomena involved in the self-assembling of functionalized cyclized backbone is an important step to developing novel self-assembly cyclic peptides. During the last decade, a considerable number of publications introduced the framework for functionalization of linear SAPs to control their molecular aggregation and bioactivity.[27,60,61] The linear FAQ-LDLK12 (FAQRVPPGGGLDLKLDLKLDLK) and linear Ac-FAQ-LDLK12 (Ac-FAQRVPPGGGLDLKLDLKLDLK) were previously designed, using phage display technology as customized motifs, to be used for neural tissue regeneration. The SAPs FAQ-LDLK12 and Ac-FAQ-LDLK12 showed high biocompatibility and locomotor recovery in *in vivo* spinal cord injury (SCI) models.[27] Thus, cyclo-FAQ-LDLK12 (22 amino acids) was synthesized following the same synthesis protocol used for cyclo-LDLK12. The effects of such biofunctionalization on self-assembly and biomimetics were then investigated. Surprisingly, cyclo-FAQ-LDLK12 showed similar behavior to cyclo-LDLK12 in terms of β-content, and reversible transition of nanostructures, suggesting a general approach useful for the fabrication of cyclic peptide-based nanomaterials with fine-tuned dimensions.[62] Linear SAPs are supramolecular hydrogels characterized by tunable rheological properties. However, due to the poor rigidity, they require physical or chemical post-self-assembly modifications to overcome the typical weakness of soft materials. Furthermore, linear SAPs may undergo rapid proteolysis.[63] Cyclic peptides could overcome this limitation because they were reported to feature lower degradation and high physiological stability.[64] Thus, we investigated the rheological properties of cyclic-FAQ-LDLK12, FAQ-LDLK12 and Ac-FAQ-LDLK12 (Fig. S2, ESI†). The elastic modulus exhibited a G' of 20000 ± 932 Pa, significantly higher than FAQ-LDLK12 (186 ± 27 Pa) and Ac-FAQ-LDLK12 (126 ± 35 Pa). The executed strain-sweep measurement, moreover, revealed that cyclo-FAQ-LDLK12 showed gradual decrements of G' at high strain %, without a rapid failure.

The rheological results highlight the boosted performance, thanks to its superimposed structure, of cyclo-FAQ-LDLK12 with respect to corresponding linear SAPs.

ThT-binding assay was used, also for cyclo-FAQ-LDLK12, to investigate the β-sheets content (Fig. S3, ESI†). Although the specific fluorescent signal at 482 nm representing the interaction between the dye and the β-secondary structure[65] was quantitatively higher in linear FAQ-LDLK12 and Ac-FAQ-LDLK12 (the N-terminal capped linear counterpart), cyclo-FAQ-LDLK12 in aqueous solution manifested a still significant amount of β-sheet content compared to ThT not bound. Among cyclic peptides this fashion is rare because of their restricted conformational flexibility.[44] The literature reported that thanks to its imposition of structural constraints, a cyclized 22-mer (but not the linear 22-mer), acting as peptidomimetic of the β-amyloid (Aβ) binding epitope on transthyretin, suppressed Aβ aggregation into fibrils and showed neuroprotection against Aβ toxicity.[66]

The secondary structure was also studied through FT-IR (Fig. S4a, ESI†), Raman (Fig. S4b, ESI†), and CD analysis (Fig. S5, ESI†).

The resulting ATR-FTIR absorption spectra of cyclo-FAQ-LDLK12, were deconvoluted, showing a wide peak in the amide I band (1500–1700 cm^{-1}). Deconvolutions showed similar behavior with cyclo-LDLK12. Acidic (pH ∼ 2, Fig. S4aI, ESI†) and neutral (pH ∼ 7, Fig. S4aII, ESI†) conditions revealed peaks at ∼1660 cm^{-1} and ∼1676 cm^{-1} ascribable respectively to β-sheet and β-turn structures. The peak at ∼1622 cm^{-1} is associated with antiparallel β-sheets. In basic conditions (pH ∼ 10, Fig. S4aIII, ESI†) a major content of the β-turn and random coil is demonstrated by the peak at ∼1680 cm^{-1}. The Raman spectra confirmed the same tendency observed for cyclo-LDLK12. In fact, the strong C$_\alpha$–H stretching mode which dominates the spectra at pH ∼ 2 (Fig. S4bI, ESI†) and pH ∼ 7 (Fig. S4bII, ESI†) becomes less pronounced at pH ∼ 10 (Fig. S4bIII, ESI†), while the main bands relative to β-turns and random coil are present (Fig. S4bIII, ESI†) in accordance with FT-IR experiments. CD analysis (Fig. S5, ESI†) for cyclo-FAQ-LDLK12 contained data non-directly attributable to a β-sheets content predominance, suggesting that antiparallel β-sheets were not present in cyclo-FAQ-LDLK12. Deconvolution operations (Table S2, ESI†) revealed the presence of a mixture of secondary structure components, with a predominant β-antiparallel component, in agreement with cyclo-LDLK12 and with the other experiments.

Finally, morphological characterization with AFM showed strong evidence of supramolecular self-assembled nanostructures tunable with pH-exchange (Fig. S6, ESI†). Linear nanostructures in cyclo-FAQ-LDLK12 were observed in both acidic and neutral conditions (Fig. S6I and S6II, ESI†), showing the importance of the constrained functionalized self-assembly backbone.[61]

The AFM analysis featured a morphology transition into round-shaped aggregates (basic conditions, Fig. S7III, ESI†) with width averages significantly larger (w_1 = 69.49 ± 1.13 nm; w_2 = 212.85 ± 3.18) than in cyclo-LDLK12. The height and width profiles of cyclo-FAQ-LDLK12 in basic conditions are reported in Fig. S7 (ESI†). It can be observed that all

nanostructures were converted into round aggregates in a rapid and reversible process. According to similar studies reported in the literature of cyclic peptides,[67] the linear nanostructures and round-shaped aggregates found in our AFM images (supported by spectroscopy analysis data) are likely nanotubes/nanofibers and nanovesicles respectively; however, further structural investigations, *i.e.* cryo-TEM and NMR, are required to confirm this hypothesis. In our previous works,[27,68] linear functionalized FAQ-LDLK12 SAP was tested *in vitro* with hNSCs and its biomimetic properties were demonstrated by the supporting cell viability assay. Here, we evaluated if peptide cyclization could affect, above all, viability of hNSCs. It is well-known that many naturally-derived cyclic peptides have anticancer, antibacterial, antifungal, and antibiotic properties, exhibiting remarkable *in vitro* cytotoxicity against numerous types of cells:[68–70] some of them act as potent growth inhibitors, with apoptotic effects against numerous human cancer cell lines.[71] Indeed, compared to linear peptides, cyclic peptides have better biological activity and an increased selectivity toward target molecules, due to the structural rigidity of their conformation. This peculiar characteristic increases their biochemical stability, binding affinity, and cell membrane permeability, making them suitable for therapeutic applications.[72,73] hNSCs were seeded on the top-surface of cyclo-FAQ-LDLK12, with Cultrex as the gold-standard and untreated glass as the negative control. The percentage of $70.73 \pm 1.88\%$ of live cells revealed a reduction in cell viability for hNSCs on cyclo-FAQ-LDLK12, compared to Cultrex ($86.95 \pm 1.33\%$, $***p < 0.001$) and to the negative control ($75.67 \pm 0.57\%$, $*p < 0.05$) (Fig. 5g). However, $29.27 \pm 1.88\%$ of dead cells show the moderate cytotoxicity of cyclo-FAQ-LDLK12. Cyclo-FAQ-LDLK12 did not completely affect the viability of hNSCs and could be considered as a biocompatible substrate for hNSCs, inspiring the development of additional novel cyclic SAPs.

Ultimately, we further investigated the potential resistance of cyclo-LDLK12 and cyclo-FAQ-LDLK12 to hydrolysis. A microwave-assisted acid hydrolysis in the presence of HCl and with the strong conditions of 80 °C, 300 W was used, followed by LC-MS analysis for the quantification of the non-hydrolyzed amount.[74] As expected both cyclo-LDLK12 and cyclo-FAQ-LDLK12 were shown to be more resistant to hydrolysis than their linear counterparts (Fig. S8 and Table S3, ESI†), emphasizing how cyclization stabilizes their structures, suggesting their usage in physiological environments where proteases resistance is required by the target application.[75–77]

Experimental

Chemicals and reagents

The reagents TFA, DIPEA, 1-[bis(dimethylamino)methylene]-1*H*-1,2,3-triazolo[4,5-*b*]pyridinium 3-oxid hexafluorophosphate (HATU), *N*-[(1*H*-benzotriazol-1-yl)(dimethylamino)methylene]-*N*-methylmethanaminium hexafluorophosphate *N*-oxide (HBTU), PyBOP, HOBt, acetic anhydride (Ac₂O), and solvents dichloromethane (DCM), *N*,*N*-dimethylformamide (DMF), 3,6-dioxa-1,8-
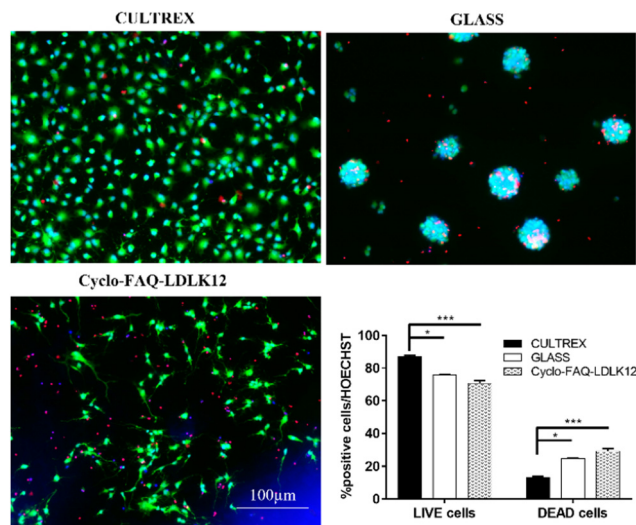

Fig. 5 Viability assessment of hNSC seeded on Cyclo-FAQ-LDLK12. The graph shows the negligible cytotoxic effect ascribable to Cyclo-FAQ-LDLK12 (LIVE/DEAD viability/cytotoxicity assay). In representative images live cells are stained in green, dead cells in red. Cell nuclei are counter-stained with Hoechst. Cultrex is considered as gold-standard, untreated glass as negative control. Statistical analyses reveal significant differences between groups with $*p < 0.05$ and $***p < 0.001$. Scale bar, 200 μm.

octanedithiol (DODt), methanol (MeOH), diethyl ether (Et₂O), ethanol (EtOH), acetonitrile (ACN), *N*-methyl-2-pyrrolidinone (NMP), and triisopropylsilane (TIS) were purchased from commercial suppliers and used without further purification. 2-Chlorotrityl chloride resin (2-CTC, 100–200 mesh, 1% DVB) was obtained from Merck (Merck Millipore, Darmstadt, Germany). All Fmoc-protected amino acids and Rink amide resin were obtained from CEM (Matthews, NC, USA). The structure, identity, and purity of intermediates and final products were verified through single quadrupole mass detection (Waters LC-MS Alliance 3100, Waters Corp., Milford, CT, USA) using nebulizing nitrogen gas at 400 L min⁻¹ and a temperature of 250 °C, cone voltage 60 V, capillary 3.5 kV, and cone flow 40 mL min⁻¹, or with a Waters ACQUITY UPLC system (Waters Corp., Milford, CT, USA) coupled with a Waters Xevo G2-XS QT of a mass spectrometer in a positive mode using a temperature of 150 °C, cone voltage 20 V, capillary 3 kV, and cone flow 20 mL min⁻¹.

General procedure for the synthesis of cyclo-LDLK12 and cyclo-FAQ-LDLK12

Fmoc-solid-phase chemistry was used for the synthesis of the linear precursors using a CEM Liberty Blue system (CEM Corp., Matthews, NC, Canada). on a 0.25 mmol scale, under a coupling condition of 1 M DIC in DMF and 1 M Oxyma in DMF. The linear precursors for cyclic peptides were synthesized using a 2-CTC resin (Scheme S1, ESI†). After loading of the first amino acid (50 W, 30 minutes, 50 °C), the resin was quenched in the presence of DIPEA/MeOH/DCM 5 : 15 : 80. All Fmoc-protected amino acids were dissolved in DMF and deprotected with a 10% v/v of piperazine in 90 : 10 NMP/EtOH solution. The cleavage from the resin, with the protecting groups intact, was performed with a

mild condition of 1% TFA in DCM, and the reaction was carried out for 1 h at room temperature (RT). The resin was then filtered in a 10% pyridine in MeOH solution (3 mL) and the residual protected peptide was washed from the resin with DCM. The combined filtrates were evaporated under reduced pressure and the crude product was precipitated in the presence of Et$_2$O. After centrifugation and decantation of the supernatant, the obtained peptide 3 (Scheme S1, ESI†) was lyophilized (Labconco, Kansas City, MO, USA). To perform the head-to-tail cyclization, a solution of DIPEA (200 μL, 0,4 mmol) was added in a glass vial to a solution of 0,1 mmol of crude 3 (Scheme S1, ESI†) dissolved in 5 mL of NMP. PyBop (0.2 mmol) and HOBt (0.2 mmol) were dissolved in 1 mL of NMP and the resulting solution was added dropwise to the glass vial over 60 minutes and the reaction was stirred at RT. After 6 hours, the solvent reaction was removed under reduced pressure, and the vial was left overnight under high vacuum. The obtained crude product 4 (Scheme S1, ESI†) was treated with 5 mL of 1:1 TFA/DCM for 2 hours at RT for the side-chains deprotection. Thus, a solution of Et$_2$O was added to precipitate the product. After centrifuge, the crude material was lyophilized. Purification of the crude product was carried out *via* flash chromatography (eluent: MeOH/DCM 5/95) and the isolated peptide was used for further characterization.

General procedure for the synthesis of linear peptides

Linear peptides FAQ-LDLK12 and Ac-FAQ-LDLK12 were synthesized with a CEM Liberty Blue synthesizer (CEM Corp., Matthews, NC, Canada) on a 0.25 mmol scale and using 0,19 Rink Amide resin. The coupling reaction was performed in the presence of 1 M DIC in DMF as an activator and 1 M oxyma in DMF as the activator base. Fmoc groups were removed with a solution of 10% v/v of piperazine in 90:10 NMP/EtOH. The acetylation of the N-terminal group was performed using a 20% v/v solution of Ac$_2$O in DMF. Cleavage from the resin was then performed using a TFA:H$_2$O:DODt:TIS (92.5:2.5:2.5:2.5) cocktail solution in a CEM RAZOR System (CEM Corp., Matthews, NC, Canada). The resin was then filtered and the TFA solution was added into cold Et$_2$O to precipitate the crude peptide, that were further lyophilized (Labconco, Kansas City, MO, USA). The desired peptide was purified by a semi-preparative Waters binary HPLC using a C18 Restek™ (Restek Corp., Bellefonte, PA, USA) column. The mobile phase consisted of solvents (A) H$_2$O:TFA (99.9:0.1) and (B) ACN:TFA (99.9:0.1) with a gradient of 25% (B) (0 min) to 100% (B) (30 min).

pH-exchange protocol

This pH-exchange protocol is a revised version of the method reported by Sun *et al.*[62] The cyclic peptide was dissolved in a glass vial with deionized water at the concentration of 1% w/v, and then completely solubilized with 25 mM NaOH until pH ~ 10 (basic solution). Thus, a solution of 10 mM TFA was added dropwise to the basic solution previously prepared until a pH ~ 7 (neutral solution). Finally, TFA 10 mM was added to the neutral solution reaching a pH ~ 2. The three solutions were capped and left 48 hours at room temperature. Finally, they were used as such for further investigations.

AFM

AFM images were captured in tapping mode with a Multimode Nanoscope V (Digital Instruments, Veeco, Plainview, NY, USA), using a single cantilever beam probe (Veeco RFESP MPP-21100-10, cantilever f0, 76–90 kHz). After image capturing, a first-order flattening was applied to data sets. Measured objects were corrected *via* the corrector formula due to the convolution effect arising from the finite size of the AFM tip. The observed heights and widths profiles from nanofibers and nanotubes were corrected with the formula:

$$x = \sqrt{2[h(2r_{t} - h)]}$$

where Δx is the width broadening effect, h is the nanofiber height, and r_{t} is the tip radius. AFM images were traced using FiberApp software.[78] While the nanosphere measurements were corrected with the formula:[79]

$$D' = \sqrt{D^2 - 8hr_{t}}$$

where D and h are the width and height of the nanosphere and r_{t} is the radius of the AFM tip. All initial sample concentrations were 1% (w/v) and the solution was diluted to a final concentration of 0.001% w/v right before imaging. 1 μL was deposited on freshly cleaved mica and rinsed with 100 μL of distilled water.[80]

ThT binding assay

ThT analyses were performed to evaluate the content of β-sheets[81] in linear and cyclic SAPs. In 1-cm-path-long micro-fluorescence cells, ThT solution was added to the peptide solutions in a ratio 0.5:1, and the mixture was stirred for 3 min. The ThT binding assay was evaluated by the use of an Infinite M200 Pro plate reader (Tecan, Mennedorf, Switzerland) with excitation at 440 nm and emission at 482 nm. The emission fluorescence spectra were recorded from 460 to 600 nm and graphs were processed using Origin™ 8 software (OriginLab Corporation, Northampton, MA, USA).

ATR/FTIR analysis

ATR/FTIR spectra were collected using a PerkinElmer Spectrum Two IR spectrometer (PerkinElmer Ltd, Beaconsfield, United Kingdom) equipped with a PerkinElmer single-reflection diamond ATR. All spectra were collected in the range of 400 to 4000 cm^{-1} at RT, and amide I and amide II regions were evaluated. The spectra were elaborated by using Origin™ 8 software. Firstly, a baseline correction was performed, and hidden peaks were detected using a second derivative method followed by smoothing with the 7–9 point Savitsky–Golay function with a polynomial order of 2. Peak deconvolution was then performed using the Voigt function[82] from OriginPro which is the convolution of a Gaussian function and a Lorentzian function.[82,83]

Raman spectroscopy

Micro-Raman measurements were carried out at RT using a confocal LabRAM (Horiba Jobin-Yvon, France) spectrometer, operating in backscattering configuration, and equipped with a BX40 microscope head (Olympus, Japan) and focusing a helium-neon laser working at 633 nm by a Long Working

Distance 10× objective with a Numerical Aperture of 0.25. The scattered light was detected by a charge-coupled device (CCD-Sincerity, JobinYvon). Samples were deposited on silicon substrates and the measure was collected after complete evaporation of water. Each experiment was performed in triplicate.

CD

CD studies were carried out on a Jasco J-810 (Jasco Corp., Tokyo, Japan) spectropolarimeter using a 1 mm path length quartz cuvette. Spectra were collected in the far-UV spectral range at room temperature, and at a scan speed of 10 nm min^{-1} with the bandwidth and time–response parameters set to 2 nm and 0,5 s, respectively. The measurements were acquired at 0.01 mg mL^{-1} peptide concentration in water, followed by a consecutive pH exchange. Data were analysed by using the software Spectra Manager version 1.55.00. CD deconvolution was performed according to the literature using Spectra deconvolution version 2.1.[51]

Rheological characterization

Rheological analysis was performed at +25 °C using a controlled stress rheometer (AR-2000ex, TA instruments) with a truncated acrylic cone-plate geometry (truncation gap, 34 μm; diameter, 20 mm; angle, 1%). Elastic modulus (G') and loss modulus (G'') were evaluated in frequency-sweep tests and recorded as a function of angular frequency (0.1–100 Hz) at a fixed strain of 1%. Tests were performed after 3 h-long time-sweeps (constant angular frequency of 1 Hz) immediately after pH shifts, to assess self-assembling. All linear peptides were dissolved in deionized water at the concentration of 1% w/v, while cyclo-FAQ-LDLK12 was tested at the concentration of 0.5% w/v.

Partial hydrolysis

Linear (LDLK12 and FAQ-LDLK12) and cyclic (cyclo-LDLK12 and cyclo-FAQ-LDLK12) peptides were treated under strong conditions to test their resistance to hydrolysis.[74] by the use of a microwave-assisted acid hydrolysis. A 0.1 mg mL^{-1} peptide was added to a 1.5 mL centrifuge tube in the presence of 3 M HCl, and then, placed in a reaction vessel of a microwave system (CEM Corp., Matthews, NC, Canada). Each sample was left for 12 min at 80 °C, 300 W for HCl hydrolysis, followed by MS analysis (Waters LC-MS Alliance 3100, Waters Corp., Milford, CT, USA). In particular, the partially hydrolyzed peptide was filtered using a 0.2 μm filter (Sartorius) and diluted with a solution of 0.1% formic acid (FA) in H$_2$O. The resulting peptide solution was loaded onto a Waters electrospray ionization MS system (Waters) using an XBridge column (C18, 2.5 μm, 2.1 × 50 mm, Waters). Chromatograms were obtained with (A) H$_2$O : FA (99.9 : 0.1) and (B) ACN : FA (99.9 : 0.1) mobile phases with a gradient of 25% (B) (0 min) to 100% (B) (5 min). A calibration curve was prepared for the quantification process by the use of a series of working solution of each peptide (Fig. S2, ESI†). Peak quantifications were, then, processed with MassLynx™ software (Table S3, ESI†).

Cell viability assays

hNSCs were obtained according to good manufacturing practice (GMP) protocols, in agreement with the European Medical Agency (EMA) guidelines and Agenzia Italiana del Farmaco (AIFA), protocol number aM 101/2010 (updated in 2018 after AIFA inspection to number aM 54/2018). Human brain tissue, derived from the forebrain, was routinely collected from spontaneous miscarriages at gestational age greater than the 8th post-conceptional week, upon the mother giving informed consent. hNSCs were expanded and cultured as previously described.[68] Cell viability and differentiation assays were performed for cyclo FAQ-LDLK12. This peptide, previously dissolved at 0.5% w/v in distilled water (GIBCO), was assembled into a 48 well multiwell (30 μL for each well). hNSCs were seeded on the top surface at density of 3 × 10^4 cells cm^{-2} and then cultured for 7 days *in vitro*. Cultrex-BME substrate and untreated-bottom well surface (namely glass) were used as gold standard and negative control, respectively. hNSCs were differentiated for the first two days in the basal medium supplemented with basic fibroblast growth factor (bFGF, 10 ng mL^{-1}). Afterwards, the bFGF medium was shifted to basal medium supplemented with leukemia inhibitory factor (LIF, 20 ng mL^{-1}) (Merck) and a brain derived neurotrophic factor (BDNF, 20 ng mL^{-1}) (Peprotech). Fresh medium was replaced after 3 days. Cell cultures were maintained at 37 °C, 20% O$_2$ and 5% CO$_2$ to support cell differentiation. After 7 days, LIVE/DEAD™ viability/cytotoxicity Kit (Invitrogen, ThermoFisher) was used to stain live cells in green with Calcein-AM, and dead cells in red with Ethidium homodimer-1. Cell nuclei were stained with Hoechst (1 : 500). Fluorescence images were acquired using a Zeiss microscope ApoTome System. Quantitative analyses were performed by counting manually positive cells for each marker using NIH-ImageJ software. Three independent experiments were performed. Statistical analysis was performed using Graph-Pad Prism 7. One-way ANOVA followed by a Turkey multiple comparison test was used to determine statistical significance (*$p < 0.05$). All experiments were conducted in triplicate.

Computational details

The configurations of cyclo-LDLK12 peptides were generated by Pymol (https://pymol.org), the script gmx_makecyclictop (https://github.com/visvaldask/gmx_makecyclictop) and mapped according to the MARTINI model. At neutral pH, arginine, lysine, and aspartic acid side chains, because of their weak basic and acidic nature, can be considered fully protonated and deprotonated respectively. Peptides have been randomly distributed in explicit water cubic boxes built by using PACKMOL in order to have the correct spatial distribution of the monomers.[84] Atoms belonging to different peptides were placed at a minimum distance of 10 Å from each other (Table S4 for details, ESI†).

United atom MD

Due to the lack of accurate structural information about cyclo-LDLK12 peptides, the self-assembly process of this SAP class has been investigated by means of more accurate UA-MD simulations. The simulation details of Cyclo-LDLK12 SAPs are shown in Table S4 (ESI†). Arginine and lysine residues are in the protonated state. The monomers have been embedded in a box of explicit water and submitted to three simulations of

50 ns each with different initial velocity distributions. A distance of 10 Å has been left between the peptides and the box edges to preserve the minimum image convention. The initial configurations of the multi-peptide systems were prepared by insertion of variable counts of monomers in random orientations and positions in cubic boxes filled by explicit water so that atoms belonging to different peptides were at least 10 Å away from each other.[85] Molecular dynamics were run using version 4.5.5 of the GROMACS simulation package and the GROMOS53a6 force field.[85,86] Prior to the production phase, the systems underwent an equilibration phase consisting in the following steps: steepest descent minimization first in a vacuum then in water and ions, a brief simulation in the *NVT* ensemble with 2 fs time-step, position restrained peptides and the temperature fixed at 310 K. The production phase was conducted in the *NPT* ensemble. Solutes and solvent were coupled independently to an external bath (T = 310 K) with a coupling constant (τ_T) of 0.1 ps using a v-rescale thermostat. Periodic boundary conditions were imposed, and pressure was maintained at 1 bar using the Berendsen coupling.[87] The isothermal compressibility was set at 4.5×10^{-5} bar^{-1} and the coupling constant (τ_P) was 0.1 ps. The constraints on lengths and angles of the bonds were applied with the LINCS algorithm. All systems were simulated as indicated in Table S4 (ESI†) using an integration time-step of 2 fs, while snapshots of individual trajectories were saved every 10 fs.

MARTINI coarse-grained MD

In MARTINI coarse-grained molecular dynamics (CGMD) simulations it is necessary to define peptide secondary structures, and the abovementioned parameters, to which individual amino acid residues must evolve.[52] The secondary structures have been assigned as fully extended, according to the evidence obtained from experimental characterization. MD simulations were performed using version 4.5.5 of the GROMACS package.[85,87] Prior to the production phase, the systems were equilibrated (a 3000-steps minimization using the steepest descents method) to eliminate high-energy interactions. The production phase was conducted in the *NPT* ensemble. Solutes and solvent were coupled independently to an external bath (T = 310 K) with a coupling constant (τT) of 1 ps using a v-rescale thermostat. Periodic boundary conditions were imposed, and pressure was maintained at 1 bar using the Berendsen coupling.[88] The isothermal compressibility was set at 3×10^{-4} bar^{-1} and the coupling constant (τ_P) was 1 ps.[89] The constraints on lengths and angles of the bonds were applied with the LINCS algorithm. All systems were simulated as indicated in Table S4 (ESI†) using an integration time-step of 20 fs, while snapshots of individual trajectories were saved every 100 fs.

Conclusions

Thanks to their high biocompatibility, low toxicity, and biomimetic properties, self-assembling peptides may be applied in multiple therapeutic areas. Recently, cyclic peptides have emerged as the most promising novel peptide therapeutics.[77,90]

As already reported in the literature, cyclization is a chemical strategy to improve peptide stability, half-life, and bioavailability. To date, only a small number of peptide sequences, comprising alternating D- and L-amino acids, have been designed to obtain cylindrical structures stabilized by non-covalent interactions. Although further studies will be required to evaluate other physical/chemical parameters, this work describes the first example of cyclic SAPs without the use of alternating D/L amino acids, yielding reversible nanostructures with predominant β-type conformation. The functionalization with the FAQ motif did not affect the self-assembling propensity of the LDLK12 backbone and yielded a more soluble cyclic peptide in aqueous solutions, allowing assessment of rheological properties and cytotoxicity. In conclusion, our results proposed an easy approach that can be applied to other linear SAPs, reaching an infinite number of novel cyclic SAP sequences, tunable with further functionalization to control biomimetics and biophysical properties (*i.e.* solubility, internal diameter, and hydrophobicity) of the self-assembling nanomaterial. All-L cyclic SAPs are a still unexplored class of peptides: therefore, by greatly enriching the diversity of cyclic peptides, they open new possibilities in different applications, such as membrane permeation, artificial ion channel, drug delivery, smart materials and molecular recognition.

Author contributions

M. G. C. performed all chemical synthesis, FT-IR, and rheological measurements, supported by E. S., all AFM measurements and analysis, and wrote the manuscript; F. F. performed the coarse-grained simulations, atomistic MD simulations, computational analysis and wrote the manuscript; R. L. performed Raman experiments with E. S. and wrote the manuscript; A. M. executed *in vitro* experiments, analyzed data, and wrote the manuscript; L. C. performed Qtof analysis; F. G. and M. G. C. designed the research concept, managed the project, and were the main contributors to the manuscript writing; A. P. reviewed the manuscript; S. S. acquired and analyzed CD spectra; F. G. supervised the project and provided funding, instruments and resources. All authors reviewed and edited the manuscript.

Conflicts of interest

There are no conflicts to declare.

References

1 D. S. Nielsen, N. E. Shepherd, W. Xu, A. J. Lucke, M. J. Stoermer and D. P. Fairlie, Orally Absorbed Cyclic Peptides, *Chem. Rev.*, 2017, **117**(12), 8094–8128, DOI: **10.1021/acs.chemrev.6b00838**.

2 J. Kisiday, M. Jin and B. Kurz, *et al.*, Self-assembling peptide hydrogel fosters chondrocyte extracellular matrix production and cell division: Implications for cartilage tissue

repair, *Proc. Natl. Acad. Sci. U. S. A.*, 2002, **99**(15), 9996–10001, DOI: **10.1073/pnas.142309999**.

3 L. Wang, N. Wang and W. Zhang, *et al.*, Therapeutic peptides: current applications and future directions, *Signal Transduction Targeted Ther.*, 2022, **7**(1), 48, DOI: **10.1038/s41392-022-00904-4**.

4 K. Fosgerau and T. Hoffmann, Peptide therapeutics: current status and future directions, *Drug Discovery Today*, 2015, **20**(1), 122–128, DOI: **10.1016/j.drudis.2014.10.003**.

5 S. Yadav, A. K. Sharma and P. Kumar, Nanoscale Self-Assembly for Therapeutic Delivery, *Front Bioeng Biotechnol.*, 2020, 8, DOI: **10.3389/fbioe.2020.00127**.

6 F. Gelain, Z. Luo and S. Zhang, Self-Assembling Peptide EAK16 and RADA16 Nanofiber Scaffold Hydrogel, *Chem. Rev.*, 2020, **120**(24), 13434–13460, DOI: **10.1021/acs.chemrev.0c00690**.

7 S. Zhang, C. Lockshin, A. Herbert, E. Winter and A. Rich, Zuotin, a putative Z-DNA binding protein in Saccharomyces cerevisiae, *EMBO J.*, 1992, **11**(10), 3787–3796, DOI: **10.1002/j.1460-2075.1992.tb05464.x**.

8 S. Zhang, T. Holmes, C. Lockshin and A. Rich, Spontaneous assembly of a self-complementary oligopeptide to form a stable macroscopic membrane, *Proc. Natl. Acad. Sci. U. S. A.*, 1993, **90**(8), 3334–3338, DOI: **10.1073/pnas.90.8.3334**.

9 T. C. Holmes, S. de Lacalle, X. Su, G. Liu, A. Rich and S. Zhang, Extensive neurite outgrowth and active synapse formation on self-assembling peptide scaffolds, *Proc. Natl. Acad. Sci. U. S. A.*, 2000, **97**(12), 6728–6733, DOI: **10.1073/pnas.97.12.6728**.

10 S. J. Choi, W. J. Jeong and S. K. Kang, *et al.*, Differential Self-Assembly Behaviors of Cyclic and Linear Peptides, *Biomacromolecules*, 2012, **13**(7), 1991–1995, DOI: **10.1021/bm3005947**.

11 D. T. Bong, T. D. Clark, J. R. Granja and M. R. Ghadiri, Self-Assembling Organic Nanotubes, *Angew. Chem., Int. Ed.*, 2001, **40**(6), 988–1011. https://doi.org/10.1002/1521-3773(20010316)40:6<988::AID-ANIE9880>3.0.CO;2-N.

12 H. Li, D. J. DeRosier, W. V. Nicholson, E. Nogales and K. H. Downing, Microtubule Structure at 8 Å Resolution, *Structure*, 2002, **10**(10), 1317–1328, DOI: **10.1016/S0969-2126(02)00827-4**.

13 S. Iijima, Helical microtubules of graphitic carbon, *Nature*, 1991, **354**(6348), 56–58, DOI: **10.1038/354056a0**.

14 T. W. Ebbesen and P. M. Ajayan, Large-scale synthesis of carbon nanotubes, *Nature*, 1992, **358**(6383), 220–222, DOI: **10.1038/358220a0**.

15 Y. Lin, S. Taylor and H. Li, *et al.*, Advances toward bioapplications of carbon nanotubes, *J. Mater. Chem.*, 2004, **14**(4), 527, DOI: **10.1039/b314481j**.

16 J. Montenegro, M. R. Ghadiri and J. R. Granja, Ion Channel Models Based on Self-Assembling Cyclic Peptide Nanotubes, *Acc. Chem. Res.*, 2013, **46**(12), 2955–2965, DOI: **10.1021/ar400061d**.

17 A. Fuertes, M. Juanes, J. R. Granja and J. Montenegro, Supramolecular functional assemblies: dynamic membrane transporters and peptide nanotubular composites, *Chem. Commun.*, 2017, **53**(56), 7861–7871, DOI: **10.1039/C7CC02997G**.

18 Y. B. Lim, E. Lee and M. Lee, Cell-Penetrating-Peptide-Coated Nanoribbons for Intracellular Nanocarriers, *Angew.*

Chem., Int. Ed., 2007, **46**(19), 3475–3478, DOI: **10.1002/anie.200604576**.

19 S. Futaki, Membrane-permeable arginine-rich peptides and the translocation mechanisms, *Adv. Drug Delivery Rev.*, 2005, **57**(4), 547–558, DOI: **10.1016/j.addr.2004.10.009**.

20 H. S. Kim, J. D. Hartgerink and M. R. Ghadiri, Oriented self-assembly of cyclic peptide nanotubes in lipid membranes, *J. Am. Chem. Soc.*, 1998, **120**(18), 4417–4424, DOI: **10.1021/ja9735315**.

21 T. Fan, X. Yu, B. Shen and L. Sun, Peptide Self-Assembled Nanostructures for Drug Delivery Applications, *J. Nanomater.*, 2017, **2017**, 1–16, DOI: **10.1155/2017/4562474**.

22 E. K. Johnson, D. J. Adams and P. J. Cameron, Peptide based low molecular weight gelators, *J. Mater. Chem.*, 2011, **21**(7), 2024–2027, DOI: **10.1039/C0JM03099F**.

23 M. Zhou, A. M. Smith, A. K. Das, N. W. Hodson, R. F. Collins, R. V. Ulijn and J. E. Gough, Self-assembled peptide-based hydrogels as scaffolds for anchorage-dependent cells, *Biomaterials*, 2009, **30**(13), 2523–2530, DOI: **10.1016/j.biomaterials.2009.01.010**.

24 X. Yan, Y. Cui and Q. He, *et al.*, Reversible transitions between peptide nanotubes and vesicle-like structures including theoretical modeling studies, *Chem. – Eur. J.*, 2008, **14**(19), 5974–5980, DOI: **10.1002/chem.200800012**.

25 I. Insua and J. Montenegro, 1D to 2D Self Assembly of Cyclic Peptides, *J. Am. Chem. Soc.*, 2020, **142**(1), 300–307, DOI: **10.1021/jacs.9b10582**.

26 H. Farrokhpour, A. Mansouri, A. R. Rajabi and A. Najafi Chermahini, The effect of the diameter of cyclic peptide nanotube on its chirality discrimination, *J. Biomol. Struct. Dyn.*, 2019, **37**(3), 691–701, DOI: **10.1080/07391102.2018.1436090**.

27 F. Gelain, D. Cigognini and A. Caprini, *et al.*, New bioactive motifs and their use in functionalized self-assembling peptides for NSC differentiation and neural tissue engineering, *Nanoscale*, 2012, **4**(9), 2946–2957, DOI: **10.1039/c2nr30220a**.

28 A. L. Sieminski, C. E. Semino, H. Gong and R. D. Kamm, Primary sequence of ionic self-assembling peptide gels affects endothelial cell adhesion and capillary morphogenesis, *J. Biomed. Mater. Res., Part A*, 2008, **87A**(2), 494–504, DOI: **10.1002/jbm.a.31785**.

29 D. Cigognini, D. Silva, S. Paloppi and F. Gelain, Evaluation of mechanical properties and therapeutic effect of injectable self-assembling hydrogels for spinal cord injury, *J. Biomed. Nanotechnol.*, 2014, **10**(2), 309–323, DOI: **10.1166/jbn.2014.1759**.

30 J. K. Tripathi, S. Pal and B. Awasthi, *et al.*, Variants of self-assembling peptide, KLD-12 that show both rapid fracture healing and antimicrobial properties, *Biomaterials*, 2015, **56**, 92–103, DOI: **10.1016/j.biomaterials.2015.03.046**.

31 H. C. Hayes, L. Y. P. Luk and Y. H. Tsai, Approaches for peptide and protein cyclisation, *Org. Biomol. Chem.*, 2021, **19**(18), 3983–4001, DOI: **10.1039/d1ob00411e**.

32 R. Pugliese, F. Fontana, A. Marchini and F. Gelain, Branched peptides integrate into self-assembled nanostructures and enhance biomechanics of peptidic hydrogels, *Acta Biomater.*, 2018, **66**, 258–271, DOI: **10.1016/j.actbio.2017.11.026**.

33 F. Gelain, Z. Luo, M. Rioult and S. Zhang, Self-assembling peptide scaffolds in the clinic, *npj Regener. Med.*, 2021, **6**(1), 9, DOI: **10.1038/s41536-020-00116-w**.

34 M. Malesevic, U. Strijowski, D. Bächle and N. Sewald, An improved method for the solution cyclization of peptides under pseudo-high dilution conditions, *J. Biotechnol.*, 2004, **112**(1–2), 73–77, DOI: **10.1016/j.jbiotec.2004.03.015**.

35 S. Wen, K. L. Carey, Y. Nakao, N. Fusetani, G. Packham and A. Ganesan, Total synthesis of azumamide A and azumamide E, evaluation as histone deacetylase inhibitors, and design of a more potent analogue, *Org. Lett.*, 2007, **9**(6), 1105–1108, DOI: **10.1021/ol070046y**.

36 J. N. Lambert, J. P. Mitchell and K. D. Roberts, The synthesis of cyclic peptides, *J. Chem. Soc., Perkin Trans. 1*, 2001, (5), 471–484, DOI: **10.1039/b001942i**.

37 N. Sewald and H. Jakubke, *Peptides: Chemistry and Biology*, Wiley, 2002. , DOI: **10.1002/352760068X**.

38 J. S. Davies, The cyclization of peptides and depsipeptides, *J. Pept. Sci.*, 2003, **9**(8), 471–501, DOI: **10.1002/psc.491**.

39 A. Thakkar, T. B. Trinh and D. Pei, Global Analysis of Peptide Cyclization Efficiency, *ACS Comb. Sci.*, 2013, **15**(2), 120–129, DOI: **10.1021/co300136j**.

40 P. P. Bose, A. K. Das, R. P. Hegde, N. Shamala and A. Banerjee, pH-Sensitive Nanostructural Transformation of a Synthetic Self-Assembling Water-Soluble Tripeptide: Nanotube to Nanovesicle, *Chem. Mater.*, 2007, **19**(25), 6150–6157, DOI: **10.1021/cm0716147**.

41 E. Vass, M. Kurz, R. K. Konat and M. Hollósi, FTIR and CD spectroscopic studies on cyclic penta- and hexa-peptides. Detailed examination of hydrogen bonding in β- and γ-turns determined by NMR, *Spectrochim. Acta, Part A*, 1998, **54**(5), 773–786, DOI: **10.1016/S1386-1425(98)00028-6**.

42 J. A. Smith, L. G. Pease and K. D. Kopple, Reverse Turns in Peptides and Protein, *Crit. Rev. Biochem.*, 1980, **8**(4), 315–399, DOI: **10.3109/10409238009105470**.

43 T. Miyazawa, Normal vibrations of monosubstituted amides in the cis configuration and infrared spectra of diketopiperazine, *J. Mol. Spectrosc.*, 1960, **4**(1–6), 155–167, DOI: **10.1016/0022-2852(60)90075-8**.

44 A. C. Gibbs, L. H. Kondejewski and W. Gronwald, *et al.*, Unusual β-sheet periodicity in small cyclic peptides, *Nat. Struct. Biol.*, 1998, **5**(4), 284–288, DOI: **10.1038/nsb0498-284**.

45 A. Saralegi, A. Etxeberria, B. Fernández-d'Arlas, I. Mondragon, A. Eceiza and M. A. Corcuera, Effect of H12MDI isomer composition on mechanical and physico-chemical properties of polyurethanes based on amorphous and semicrystalline soft segments, *Polym. Bull.*, 2013, **70**(8), 2193–2210, DOI: **10.1007/s00289-013-0930-3**.

46 H. T. Miles, T. P. Lewis, E. D. Becker and J. Frazier, Identification of the Amide II Band in the cis-Amide 1-Methyluracil, in Poly(U), and in Poly(A)·Poly(U), *J. Biol. Chem.*, 1973, **248**(3), 1115–1117, DOI: **10.1016/S0021-9258(19)44378-0**.

47 R. A. Shaw, A. Perczel, H. H. Mantsch and G. D. Fasman, Turns in small cyclic peptides—can infrared spectroscopy detect and discriminate amongst them?, *J. Mol. Struct.*, 1994, **324**(1–2), 143–150, DOI: **10.1016/0022-2860(94)08235-9**.

48 R. A. Shaw, H. H. Mantsch and B. Z. Chowdhry, Solvent influence on the conformation of cyclosporin. An FT-IR study, *Can. J. Chem.*, 1993, **71**(9), 1334–1339, DOI: **10.1139/v93-172**.

49 M. D. Foggia, P. Taddei, A. Torreggiani, I. National and M. Dettin, Self-Assembling P Eptides for B Iomedical a Pplications: Ir and R Aman S Pectroscopies, *Proteomics Res. J.*, 2012, 1–16.

50 S. A. Oladepo, K. Xiong, Z. Hong and S. A. Asher, Elucidating Peptide and Protein Structure and Dynamics: UV Resonance Raman Spectroscopy, *J. Phys. Chem. Lett.*, 2011, **2**(4), 334–344, DOI: **10.1021/jz101619f**.

51 S. M. Kelly, T. J. Jess and N. C. Price, How to study proteins by circular dichroism, *Biochim. Biophys. Acta, Proteins Proteomics*, 2005, **1751**(2), 119–139, DOI: **10.1016/j.bbapap.2005.06.005**.

52 F. Fontana, C. Carlino, A. Malik and F. Gelain, Morphoscanner2.0: A new python module for analysis of molecular dynamics simulations, *PLoS One*, 2023, **18**(4), e0284307, DOI: **10.1371/journal.pone.0284307**.

53 C. Y. J. Lau, F. Fontana and L. D. Mandemaker, *et al.*, Control over the fibrillization yield by varying the oligomeric nucleation propensities of self-assembling peptides, *Commun. Chem.*, 2020, **3**, 164, DOI: **10.1038/s42004-020-00417-7**.

54 F. Fontana and F. Gelain, Modeling of supramolecular biopolymers: Leading the in silico revolution of tissue engineering and nanomedicine, *Nanotechnol. Rev.*, 2022, **11**(1), 2965–2996, DOI: **10.1515/ntrev-2022-0455**.

55 A. Ghosh, T. K. Mukhopadyay and A. Datta, Two dimensional materials are non-nanotoxic and biocompatible towards cyclotides: evidence from classical molecular dynamics simulations, *Nanoscale*, 2023, **15**, 321–336, DOI: **10.1039/D2NR05096J**.

56 J. Damjanovic, J. Miao, H. Huang and Y. Lin, Elucidating Solution Structures of Cyclic Peptides Using Molecular Dynamics Simulations, *Chem. Rev.*, 2021, **121**(4), 2292–2324.

57 J. Y. Rho, H. Cox and E. D. H. Mansfield, *et al.*, Dual self-assembly of supramolecular peptide nanotubes to provide stabilisation in water, *Nat. Commun.*, 2019, **10**, 4708, DOI: **10.1038/s41467-019-12586-8**.

58 M. Kobayashi, K. Fujita, K. Matsuda and T. Wakimoto, Streamlined Chemoenzymatic Synthesis of Cyclic Peptides by Non-ribosomal Peptide Cyclases, *J. Am. Chem. Soc.*, 2023, **145**(6), 3270–3275, DOI: **10.1021/jacs.2c11082**.

59 T. He, R. Qu and J. Zhang, Current synthetic chemistry towards cyclic antimicrobial peptides, *Pept. Sci.*, 2022, **28**(6), e3387, DOI: **10.1002/psc.3387**.

60 F. Taraballi, A. Natalello and M. Campione, *et al.*, Glycine-spacers influence functional motifs exposure and self-assembling propensity of functionalized substrates tailored for neural stem cell cultures, *Front. Neuroeng.*, 2010, **3**(FEB), 1–9, DOI: **10.3389/neuro.16.001.2010**.

61 F. Gelain, A. Horii and S. Zhang, Designer self-assembling peptide scaffolds for 3-D tissue cell cultures and regenerative medicine, *Macromol. Biosci.*, 2007, **7**(5), 544–551, DOI: **10.1002/mabi.200700033**.

62 L. Sun, Z. Fan, Y. Wang, Y. Huang, M. Schmidt and M. Zhang, Tunable synthesis of self-assembled cyclic

peptide nanotubes and nanoparticles, *Soft Matter*, 2015, **11**(19), 3822–3832, DOI: **10.1039/c5sm00533g**.

63 S. Eskandari, T. Guerin, I. Toth and R. J. Stephenson, Recent advances in self-assembled peptides: Implications for targeted drug delivery and vaccine engineering, *Adv. Drug Delivery Rev.*, 2017, **110-111**, 169–187, DOI: **10.1016/j.addr.2016.06.013**.

64 E. H. M. Mohammed, S. Lohan, R. K. Tiwari and K. Parang, Amphiphilic cyclic peptide [W4KR5]-Antibiotics combinations as broad-spectrum antimicrobial agents, *Eur. J. Med. Chem.*, 2022, **235**, 114278, DOI: **10.1016/j.ejmech.2022.114278**.

65 D. Ramadhani, R. Maharani, A. M. Gazzali and M. Muchtaridi, Cyclic Peptides for the Treatment of Cancers: A Review, *Molecules*, 2022, **27**(14), 4428, DOI: **10.3390/molecules27144428**.

66 S. H. Joo, Cyclic Peptides as Therapeutic Agents and Biochemical Tools, *Biomol. Ther.*, 2012, **20**(1), 19–26, DOI: **10.4062/biomolther.2012.20.1.019**.

67 R. Hourani, C. Zhang, R. van der Weegen, L. Ruiz, C. Li, S. Keten, B. A. Helms and T. Xu, Processable Cyclic Peptide Nanotubes with Tunable Interiors, *J. Am. Chem. Soc.*, 2011, **133**, 15296–15299, DOI: **10.1021/ja2063082**.

68 A. Marchini, A. Raspa and R. Pugliese, *et al.*, Multifunctionalized hydrogels foster hNSC maturation in 3D cultures and neural regeneration in spinal cord injuries, *Proc. Natl. Acad. Sci. U. S. A.*, 2019, **116**(15), 7483–7492, DOI: **10.1073/pnas.1818392116**.

69 Q. Song, Z. Cheng, M. Kariuki, S. C. L. Hall, S. K. Hill, J. Y. Rho and S. Perrier, Molecular Self-Assembly and Supramolecular Chemistry of Cyclic Peptides, *Chem. Rev.*, 2021, **121**(22), 13936–13995, DOI: **10.1021/acs.chemrev.0c01291**.

70 R. Ribeiro, E. Pinto, C. Fernandes and E. Sousa, Marine Cyclic Peptides: Antimicrobial Activity and Synthetic Strategies, *Mar. Drugs*, 2022, **20**(6), 397, DOI: **10.3390/md20060397**.

71 Eman H. M. Mohammed, Sandeep Lohan, Rakesh K. Tiwari and Keykavous Parang, Amphiphilic cyclic peptide [W4KR5]-Antibiotics combinations as broad-spectrum antimicrobial agents, *Eur. J. Med. Chem.*, 2022, **235**, 114278, DOI: **10.1016/j.ejmech.2022.114278**.

72 D. Ramadhani, R. Maharani, A. M. Gazzali and M. Muchtaridi, Cyclic Peptides for the Treatment of Cancers: A Review, *Molecules*, 2022, **27**, 4428, DOI: **10.3390/molecules27144428**.

73 M. Abdalla and L. McGaw, Natural Cyclic Peptides as an Attractive Modality for Therapeutics: A Mini Review, *Molecules*, 2018, **23**(8), 2080, DOI: **10.3390/molecules23082080**.

74 E. Gavrish, C. S. Sit, S. Cao, O. Kandror, A. Spoering, A. Peoples, L. Ling, A. Fetterman, D. Hughes, A. Bissell, H. Torrey, T. Akopian, A. Mueller, S. Epstein, A. Goldberg, J. Clardy and K. Lewis, Lassomycin, a Ribosomally Synthesized Cyclic Peptide, Kills Mycobacterium tuberculosis by Targeting the ATP-Dependent Protease ClpC1P1P2, *Chem. Biol.*, 2014, **21**(4), 509–518, DOI: **10.1016/j.chembiol.2014.01.014**.

75 J. S. Choi and S. H. Joo, Recent Trends in Cyclic Peptides as Therapeutic Agents and Biochemical Tools, *Biomol. Ther.*, 2020, **28**(1), 18–24, DOI: **10.4062/biomolther.2019.082**.

76 S. Jun, Y. Hong, H. Imamura, B. Y. Ha, J. Bechhoefer and P. Chen, Self-Assembly of the Ionic Peptide EAK16: The Effect of Charge Distributions on Self-Assembly, *Biophys. J.*, 2004, **87**(2), 1249–1259, DOI: **10.1529/biophysj.103.038166**.

77 M. G. Ciulla and F. Gelain, Structure-activity relationships of antibacterial peptides, *Microb. Biotechnol.*, 2023, **16**(4), 757–777, DOI: **10.1111/1751-7915.14213**.

78 I. Usov and R. Mezzenga, FiberApp: An Open-Source Software for Tracking and Analyzing Polymers, Filaments, Biomacromolecules, and Fibrous Objects, *Macromolecules*, 2015, **48**(5), 1269–1280, DOI: **10.1021/ma502264c**.

79 Y. Wang, T. Lu, X. Li, S. Ren and S. Bi, Robust nanobubble and nanodroplet segmentation in atomic force microscope images using the spherical Hough transform, *Beilstein J. Nanotechnol.*, 2017, **8**, 2572–2582, DOI: **10.3762/bjnano.8.257**.

80 H. Yokoi, T. Kinoshita and S. Zhang, Dynamic Reassembly of Peptide RADA16 Nanofiber Scaffold, *Proc. Natl. Acad. Sci. U. S. A.*, 2005, **102**, 8414–8419, DOI: **10.1073/pnas.0407843102**.

81 C. Xue, T. Y. Lin, D. Chang and Z. Guo, Thioflavin T as an amyloid dye: fibril quantification, optimal concentration and effect on aggregation, *R. Soc. Open Sci.*, 2017, **4**(1), 160696, DOI: **10.1098/rsos.160696**.

82 H. O. Di Rocco, D. I. Iriarte and J. Pomarico, General Expression for the Voigt Function That is of Special Interest for Applied Spectroscopy, *Appl. Spectrosc.*, 2001, **55**(7), 822–826, DOI: **10.1366/0003702011952839**.

83 Y. Ji, X. Yang and Z. Ji, *et al.*, DFT-Calculated IR Spectrum Amide I, II, and III Band Contributions of N-Methylacetamide Fine Components, *ACS Omega*, 2020, **5**(15), 8572–8578, DOI: **10.1021/acsomega.9b04421**.

84 L. Martínez, R. Andrade, E. G. Birgin and J. M. Martínez, PACKMOL: A package for building initial configurations for molecular dynamics simulations, *J. Comput. Chem.*, 2009, **30**(13), 2157–2164, DOI: **10.1002/jcc.21224**.

85 D. Van Der Spoel, E. Lindahl, B. Hess, G. Groenhof, A. E. Mark and H. J. C. Berendsen, GROMACS: Fast, flexible, and free, *J. Comput. Chem.*, 2005, **26**(16), 1701–1718, DOI: **10.1002/jcc.20291**.

86 Z. Cao, Z. Lin, J. Wang and H. Liu, Refining the description of peptide backbone conformations improves protein simulations using the GROMOS 53A6 force field, *J. Comput. Chem.*, 2009, **30**(4), 645–660, DOI: **10.1002/jcc.21092**.

87 D. H. de Jong, G. Singh and W. F. D. Bennett, *et al.*, Improved Parameters for the Martini Coarse-Grained Protein Force Field, *J. Chem. Theory Comput.*, 2013, **9**(1), 687–697, DOI: **10.1021/ct300646g**.

88 H. J. C. Berendsen, J. P. M. Postma, W. F. van Gunsteren, A. DiNola and J. R. Haak, Molecular dynamics with coupling to an external bath, *J. Chem. Phys.*, 1984, **81**(8), 3684–3690, DOI: **10.1063/1.448118**.

89 G. Bussi, D. Donadio and M. Parrinello, Canonical sampling through velocity rescaling, *J. Chem. Phys.*, 2007, **126**(1), 014101, DOI: **10.1063/1.2408420**.

90 S. Jun, Y. Hong, H. Imamura, B. Y. Ha, J. Bechhoefer and P. Chen, Self-Assembly of the Ionic Peptide EAK16: The Effect of Charge Distributions on Self-Assembly, *Biophys. J.*, 2004, **87**(2), 1249–1259, DOI: **10.1529/biophysj.103.038166**.